International Journal of Nanomedicine

Dovepress
Taylor & Francis Group

Open Access Full Text Article

ORIGINAL RESEARCH

Intervening Non-Small-Cell Lung Cancer Progression by Cell Membrane Coated Platycodin D via Regulating Hsa-miR-1246/FUT9/GSK3β Pathway

Shuyu Zheng[1,2], Zejuan Xie[1], Ziao Zhou[1], Shanshan Wang[1], Yanlin Xin[1], Jiamin Lin[1], Keyu Cheng[1], Tianming Lu[1], Ruogu Qi[1], Yuanyuan Guo[1]

[1]Department of Biochemistry and Molecular Biology, School of Medicine & Holistic Integrative Medicine, Nanjing University of Chinese Medicine, Nanjing, 210023, People's Republic of China; [2]Department of Neurosurgery, The Second Affiliated Hospital, Zhejiang University, Hangzhou, Zhejiang Province, 310009, People's Republic of China

Correspondence: Ruogu Qi; Yuanyuan Guo, Department of Biochemistry and Molecular Biology, School of Medicine & Holistic Integrative Medicine, Nanjing University of Chinese Medicine, Nanjing, 210023, People's Republic of China, Email rqi@njucm.edu.cn; guoyy@njucm.edu.cn

Purpose: Metastatic non-small cell lung cancer (NSCLC) remains a global health threat, with patients facing inevitable disease progression despite standard-of-care therapy. Prior studies showed Platycodin D (PD)-induced cell cycle arrest and apoptosis in NSCLC via RNA regulatory network, yet elucidating PD's mechanisms in NSCLC progression is challenging in the real world.

Methods: Biological effects of PD on NSCLC cell lines A549 and PC-9 were assessed through in vitro assays, encompassing apoptosis, proliferation, colony formation, migration and invasion. MicroRNAs (miRNAs) expression was profiled, and their roles were investigated using miRNA mimics or inhibitors. Predicted miRNA targets were validated via dual-luciferase reporter assays and Western blotting following bioinformatic prediction. PD's metastatic inhibitory potential in NSCLC was evaluated in an in vivo lung cancer metastasis model. Furthermore, a homologous cell membrane-based PD delivery system was established to improve the biosafety and efficacy of PD in vivo.

Results: Hsa-miR-1246 was upregulated by PD treatment, and functional experiments demonstrated that the miR-1246-mimic enhanced PD's suppressive effects on NSCLC cell proliferation, colony formation, migration, and invasion, while the miR-1246-inhibitor abrogated these effects. Notably, dual-luciferase assays confirmed that hsa-miR-1246 directly targeted the 3' untranslated regions (3' UTRs) of Fucosyltransferase 9 (FUT9), modulating its expression. Moreover, the hsa-miR-1246/FUT9 axis regulated the phosphorylation level and expression of GSK3β protein. In vivo, PD encapsulated in homologous cell membranes mitigated tumor growth and migration in metastatic NSCLC mice with minimal side effects.

Conclusion: The application of PD prompted an increase in the expression levels of hsa-miR-1246 and a concurrent decrease in FUT9. Importantly, the therapeutic efficacy of PD in vivo was markedly enhanced through homologous cell delivery system. Collectively, this study revealed the potential utility of PD in the treatment of NSCLC progression.

Keywords: non-small cell lung cancer, platycodin D, anti-cancer phytomedicine, hsa-miR-1246, FUT9, cancer cell membrane

Introduction

Lung cancer is among the deadliest cancers worldwide, with approximately 85% of cases being non-small cell lung cancers (NSCLCs).[1,2] Extensive clinical data have shown that poor patient prognosis is closely linked to tumor metastasis and recurrence. The standard treatments for NSCLC include surgery, chemotherapy and radiotherapy.[3–5] However, long-term chemotherapy use can lead to various adverse effects, such as hepatotoxicity, cardiotoxicity, and chemoresistance. Therefore, bioactive compounds from natural sources, specifically phytomedicines, are considered potential therapeutics to address these limitations and exhibit multi-targeted antitumor activities.[6–10]

Received: 24 May 2024
Accepted: 28 January 2025
Published: 6 February 2025

Platycodin D (PD), a major bioactive monomer derived from Platycodon grandiflorum (P. grandiflorum), is a traditional herbal medicine used for pulmonary diseases and respiratory disorders.[11,12] PD has been previously reported as a potent antiproliferative, antitumorigenic, and immunoregulatory agent that inhibits tumor growth and metastasis in various human cancers, including NSCLC.[13–17] Our previous network pharmacology study suggested that PD can inhibit cell growth and arrest the cell cycle in NSCLC cells by regulating the intracellular non-coding RNA network.[18] However, further in-depth research on PD's effectiveness and mechanism in NSCLC progression, both in vitro and in vivo, is scarce.

MicroRNAs (miRNAs) are small endogenous non-coding RNAs that negatively regulate target genes by binding to complementary sequences in target mRNAs, leading to mRNA degradation or translational suppression.[19–21] Numerous miRNAs are implicated in disease progression. For instance, Edmonds and Zhu et al found that miR-31-5p influences the Warburg effect in lung cancer initiation and metastasis.[22,23] In addition, miR-1-3p has been extensively studied for its role in tumor proliferation, autophagy, and migration. It targets genes such as CCL2, PRC1, and c-MET to influence tumor migration and participates in pulmonary vascular remodeling through the SPHK1 gene.[24–26] Besides, GSK3β is a critical regulator of tumor growth and metastasis. It can suppress the Wnt/β-catenin signaling pathway, generally inhibiting tumor metastasis. Conversely, GSK3β is a target of PI3K/Akt-mediated phosphorylation, and Akt activation could promote cell growth and survival by inactivating GSK3β. However, the roles of miRNAs and GSK3β in NSCLC regulated by PD have not been well characterized.[27,28]

In this study, we aimed to investigate the therapeutic potential of PD on NSCLC progression both in vitro and in vivo, and to elucidate molecular and cellular mechanisms by which miRNAs control metastasis. We conducted in vitro experiments to assess drug toxicity, cell apoptosis, proliferation, colony formation, migration, and invasion in lung cancer cells treated with PD. We also analyzed miRNA expression profiles and used miRNA mimics or inhibitors to study their functions in lung cancer cells. The downstream pathways were explored using luciferase reporter assays and Western blotting based on bioinformatic predictions of miRNA target genes. Finally, we evaluated the efficacy of PD against NSCLC metastasis using an in vivo lung cancer metastasis model. To test its biosafety and efficacy in vivo, we established a homologous cell membrane PD carrier system. These findings shed light on the anticancer phytomedicine PD's role in controlling NSCLC metastasis.

Materials and Methods

Materials

PD was purchased from Yuanye Co. Ltd. (Shanghai, China), dissolved in sterilized water to 10 mM, aliquoted, and stored at −20 °C until use. The primary antibodies used for Western blotting, immunofluorescence (IF), and immunohistochemistry (IHC) are described in Supplementary Table S1.

Animals

BALB/c nude mice (male, 4–5 weeks old) were purchased from GemPharmatech Laboratory Animal Technology (Nanjing, China) and maintained in a pathogen-free (SPF) environment. All animal studies were conducted in accordance with the approved guidelines of the Animal Care and Use Committee of the Nanjing University of Chinese Medicine (012071001744).

Cell Culture

The human lung cancer cell lines A549 and PC-9 were purchased from the cell bank of the Chinese Academy of Sciences and cultured in Dulbecco's modified Eagle's medium (DMEM) supplemented with 10% fetal bovine serum (FBS) and 1% penicillin–streptomycin at 37 °C in a humid atmosphere with 5% CO_2.

Bioinformatic Sequencing and Analysis

Sample treatment, RNA extraction, library construction, and RNA sequencing were performed as described previously. Differentially expressed miRNAs and mRNAs were identified in the control and treatment groups using R package (edgeR 3.14.0). Log2 fold change >1 and adjusted P-value <0.05 were set as the filter criteria for significant differential expression.[29,30]

Evaluation and Validation of miRNAs

To validate the expression of these miRNAs and mRNAs, real-time qPCR was performed using ChamQ Universal SYBR Green Master Mix (Vazyme, Nanjing, China) in a QuantStudio Real-Time PCR System (ThermoFisher, USA). The primer sequences are listed in Supplementary Table S2. Data were quantified using the $2^{-\Delta\Delta CT}$ method and normalized to the internal reference gene, U6.

Plasmid Construction and Luciferase Reporter Assays

To perform the luciferase reporter assay, 3' untranslated regions (3' UTRs) containing the hsa-miR-1246 binding sites of Fucosyltransferase 9 (FUT9) were amplified and inserted into the pGL3-control vector (Promega, Madison, WI, USA). Site-directed mutagenesis of the hsa-miR-1246 seed sequence in the FUT9 3'-UTR (Mut) was performed using a QuikChange Site-Directed Mutagenesis Kit (Stratagene, San Diego, CA, USA). Subsequently, HUVEC were transfected with wild-type or mutant reporter plasmids, and luciferase activity was evaluated 48 h later using the Dual-Luciferase Reporter Assay System (Promega). Full-length FUT9 cDNA lacking the 3'-UTR was purchased from GeneCopoeia (Rockville, MD, USA) and subcloned into eukaryotic expression vector pcDNA.3 (Thermo Fisher Scientific).

Proliferation, Cell Migration and Invasion Assays

Cell proliferation was measured using the CCK-8 assay. The number of live cells was determined according to the manufacturer's protocol. Briefly, after hsa-miR-1246 mimics or NC were transiently transfected into A549 or PC-9 cells, the cells were cultured in 96-well plates at a density of 2×10^4 cells/well under the culture conditions described above for 48 or 72 h. each well were added with 10μL CCK-8 solution incubating for another 1 hour. The optical density (OD) of the cells in each well was measured at 450 nm using an enzyme-linked immunosorbent assay (ELISA) plate reader (Bio-Rad, CA, USA).

The invasion and migration potential of A549 and PC-9 cells was evaluated using Transwell cell matrigel migration and invasion assays. The invasion assay was performed using Transwell chambers (8 μm pore; Corning, NY, USA) coated with Matrigel (BD Biosciences, Bedford, MA, USA). Cells were starved overnight in DMEM containing 0.1% FBS and added to the upper chambers of a 24-well plate at a concentration of $2x10^4$/chamber. The lower chambers were filled with 500μL DMEM medium supplemented with 10% FBS. After 48 h of incubation, the filters in the Transwell chambers were washed with phosphate buffered saline (PBS), fixed with methanol for 1 min, and stained with 0.5% crystal violet. The cells on the underside of the filters were counted under a light microscope (Olympus, Japan) at 100x magnification with an average count of five visual fields. The cell migration assay procedure was similar to the method described above, except that the Transwell chambers were not coated with Matrigel and the starved cells were incubated for 24 h.

To study directional cell migration, we performed a wound-healing study. A549 or PC-9 cell lines were seeded at confluence in 6-well plates. After 12 h, necessary for adhesion, a scratch was performed in the middle of each well. After washing the cells, new medium was added, and pictures of each well were taken every 24 h. The effect on cell migration was quantified by ImageJ software. Experiments were performed three times in triplicate.

Experimental Lung Metastasis Mouse Models

Five-to-six-week-old male BALB/c nude mice were purchased from Jicui Laboratory Animal Technology (Nanjing, China) and adaptively fed for at least one week before the experiments. Experimental lung metastasis mouse models were established by the intravenous (iv) injection of A549 cells. Briefly, each mouse was inoculated with A549-luc cells (5×10^6) suspended in 100 μL saline via tail vein injection. Tumor growth was monitored by bioluminescence imaging after the injection of D-luciferin potassium salt solution (150 mg/kg, intraperitoneally) 5 min post-anesthesia using an IVIS® Spectrum In Vivo Imaging System, and normalized to the same exposure time.

PD Administration

Mice showing similar lung bioluminescence signal intensities were divided randomly into different treatment groups, and were subjected to 7.5 mg/kg PD, 15 mg/kg PD, 7.5 mg/kg PD@A549-m, 15 mg/kg PD@A549-m or control treatments (intraperitoneal injection, 3 times per week for 3 weeks). At the end of the study, all mice were euthanized and the lungs, livers, and brains were dissected. Half of each sample was fixed with 10% formalin and subjected to hematoxylin and eosin (H&E) staining and immunohistochemistry (IHC), and the remaining sample was quickly frozen for protein or RNA extraction.

Immunohistochemistry Staining

The mouse samples were fixed in formalin and embedded in paraffin. Histological sections were prepared from the paraffin blocks, deparaffinized with xylene, and treated with high-temperature antigen retrieval in citrate buffer (0.01 M sodium citrate (pH 6.0)). Endogenous peroxidase was blocked with 0.3% hydrogen peroxide in methanol for 30 min, and sections were blocked with 10% BSA. The primary antibody was then incubated at 4 °C overnight and the secondary antibody was incubated at RT for 30 min. After washing, the sections were stained using a DAB peroxidase substrate kit (SK-4100; Vector Laboratories) until the desired intensity was achieved. The H Score was determined using the following formula: percentage of weak staining + 2 × percentage of moderate staining + 3 × percentage of strong staining, giving a range of 0–300.

Homogeneous Cell Membrane Coating and Analysis

Ultrasonic and extrusion approaches have been used to prepare membranes of lung cancer cells. First, A549 or PC-9 cells were cultured in 150 mm cell culture dishes, and 2×10^8 cells were counted. After the cells were completely digested with a cell scraper, they were centrifuged at 400 × g for 5 min (BiofugeStratos, Thermo), washed with PBS, and centrifuged at 400 × g for 5 min. Add 4 × volume of hypotonic buffer containing protease inhibitors, and shake every 15 min on ice to disrupt the cells. After 1 h, the cells were disrupted by sonication for 6 min (3s-on / 3s-off, 30% power, 1000 W). The suspension was then centrifuged machine at 15000 g at 4 °C for 30 min using a high-speed centrifuge, and the supernatant was collected and extruded through a 200 nm pore-sized polycarbonate membrane several times to obtain cell membrane fragments with a relatively uniform particle size. Finally, the fragments were aliquoted and stored at −80 °C. The particle size was measured using a DLS analyzer (Zetasizer, Malvern, UK). The morphologies were characterized by transmission electron microscope (TEM) (JEOL JEM-1230, Tokyo, Japan).

Statistical Analysis

Data are expressed as the mean ± standard deviation (SD) of triplicate experiments. Each experiment was repeated at least 3 times. Student's *t*-test or analysis of variance (ANOVA) was used to evaluate differences using the GraphPad Prism software (GraphPad Prism 9, USA). *P < 0.05; **P < 0.01; ***P < 0.001; ****P < 0.0001.

Results and Discussion

PD Inhibits NSCLC Cell Growth, Migration, and Invasion

A series of in vitro experiments were conducted to assess the effects of PD on NSCLC cells. The MTT assay (Supplementary Figure S1) showed that a 48-hour PD treatment significantly reduced the viability of NSCLC cell lines in a dose-dependent manner. Notably, the half-maximal inhibitory concentration (IC50) was higher in PC-9 cells (29±7μmol/L) than in A549 cells (11±0.95 μmol/L). Microscopic examination revealed an increase in cytoplasmic vacuoles in both A549 and PC-9 cell lines following PD treatment, suggesting the induction of autophagy (Figure 1A). Additionally, PD treatment increased apoptosis in A549 and PC-9 cells compared to the control group, as determined by Annexin V/PI staining (Figure 1B). Both plate colony formation and CCK-8 assays indicated that PD reduced NSCLC cell colony formation and inhibited cell growth by more than 50% relative to the control group (Figure 1C and D). We further investigated PD's impact on NSCLC migration and invasion. GSK3β, a key regulator in tumor growth and metastasis. Our experiments showed that PD could inhibit NSCLC cell growth, migration and invasion by upregulating

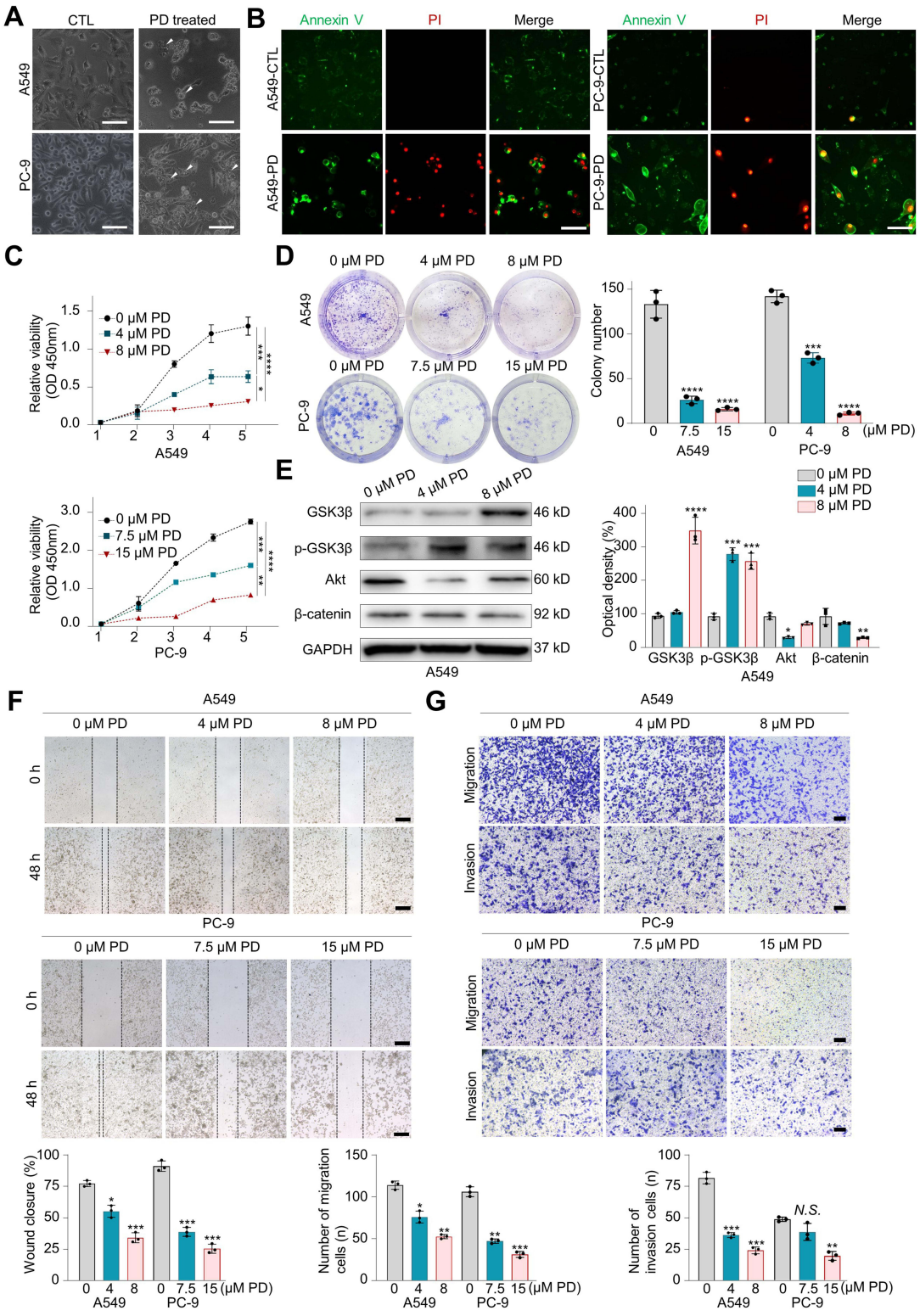

Figure 1 PD inhibits NSCLC cell growth, migration, and invasion. (**A**) Morphological changes in A549 and PC-9 cells under PD treatment with 10 μmol/L for 24h. White arrows indicate the presence of multiple vacuoles in the cytoplasm. Scale bar, 50 μm. (**B**) Annexin V/PI double staining of A549 and PC-9 cells after treatment with PD or control for 24h. Scale bar, 100 μm. (**C**) The effect of PD on cell proliferation was detected using CCK-8 assay in both A549 and PC-9 cells. N=5 for each group. (**D**) The effect of PD on colony formation in both A549 and PC-9 cells. N=5 for each group. (**E**) The effects of PD on GSK3β, phosphorylated GSK3β, Akt, and β-catenin protein expression were detected using Western blotting. (**F**) Effect of different concentrations of PD on the wound-healing function of A549 and PC-9 cells. PD at concentrations of 4μM and 8μM for A549 cells and 7.5μM and 15μM for PC-9 cells was applied to the cells for 48h. N=3 for each group. Scale bar, 200 μm. (**G**) The effect of different concentrations of PD on the migration and invasion of A549 and PC-9 cells. N=3 for each group. Scale bar, 100 μm. Data are shown as mean±SD, *P < 0.05, **P < 0.01, ***P < 0.001, ****P < 0.0001, NS, not significant.

https://doi.org/10.2147/IJN.S479675

GSK3β expression and phosphorylation, thereby inhibiting the Wnt/β-catenin and PI3K/AKT pathways compared to the control (Figure 1E). Transwell assay results indicated that PD treatment significantly impaired the migration and invasion of NSCLC cells in a dose-dependent manner (Figure 1G), a finding corroborated by the scratch wound healing assay (Figure 1F).

Identification of PD-Regulated miRNAs and Their Clinical Significance

Lung cancer metastases are characterized by their insidious onset, rapid progression, poor prognosis, and short natural survival, underscoring the urgent need for effective therapeutic interventions. Among pharmacological studies, the role of miRNAs in cancer progression has garnered significant interest. To elucidate the mechanisms by which PD inhibits NSCLC progression, we integrated in silico analysis results, including whole-transcriptome sequencing of PD-treated cells, and clinical databases (GSE 137140, GSE 38698, TCGA LUAD cohort, Figure 2F). A panel of miRNAs (hsa-miR-31-5p, hsa-miR-219-5p, hsa-miR-1-3p, hsa-miR-130a-5p, hsa-miR-452-3p, hsa-miR-598-3p, hsa-miR-1246, hsa-miR-196a-5p and hsa-miR-210-3p) were identified as common candidates regulated by PD, with the potential to distinguish metastatic NSCLC samples from primary ones (Figure 2A–C and G). To refine the list of core genes, we conducted gene ontology and KEGG pathway analyses based on the PD transcriptome data. These analyses revealed pathways crucial to the biological effects of PD on NSCLC, including cell migration, epithelial-mesenchymal transition (EMT), adherens junction, and transcriptional misregulation (Figure 2D). Notably, hsa-miR-1246 emerged as a central player and was significantly downregulated in metastatic NSCLC samples compared to controls ($P<0.001$). Furthermore, low expression of hsa-miR-1246 correlated with a poor prognosis in lung cancer patients ($P<0.0001$, Figure 2E).

PD Increases Hsa-miR-1246 Expression to Mediate Cell Growth, Migration, and Invasion

As demonstrated above, a panel of miRNAs, including hsa-miR-1246, may be strongly associated with NSCLC progression. However, it remains unclear whether they can regulate functional effects in tumor cells. Initially, we tested miRNA expression in A549 and PC-9 cells treated with different doses of PD. A consistent increase in hsa-miR-1246 expression was observed in both the cell lines following PD treatment (Figure 3A). To further investigate this, an miR-1246-mimic or inhibitor was introduced to modulate the expression of hsa-miR-1246 (Figure 3B). The results indicated that the miR-1246-mimic significantly increased hsa-miR-1246 expression compared to the negative control (NC). Consequently, reduced cell proliferation and colony formation were accompanied by inhibition of cell migration and invasion in vitro. Conversely, silencing of hsa-miR-1246 with the miR-1246-inhibitor yielded opposing results (Figure 3C–G). Furthermore, Western blotting revealed that the miR-1246-mimic enhanced the upregulation of GSK3β expression under PD treatment, while the miR-1246-inhibitor partially reversed this effect (Figure 3E). These findings support the notion that hsa-miR-1246 inhibits proliferation, migration, and invasion of NSCLC cells under PD regulation.

Hsa-miR-1246 was initially identified through high-throughput sequencing of human embryonic stem cells, and subsequent studies have elucidated its role in various cancer cell lines, where it has been shown to regulate cell cycle progression, proliferation, stemness, and drug resistance in cancer cells.[31,32] Its role in lung cancer has been a subject of debate, with conflicting reports on whether it promotes or suppresses tumorigenesis. Yang et al reported that an miR-1246-mimic enhanced the EMT characteristics in A549 cells, decreased E-cadherin expression, and increased the expression levels of Vimentin and TGF-β.[33] Additionally, Yuan et al demonstrated that after radiation therapy, the expression of miR-1246 in the exosomes from radiotherapy-resistant A549 cells was upregulated, and miR-1246 could be transferred from donor cells to recipient cells through non-exosomal pathways, thereby enhancing the proliferation and migration of recipient cells.[34] Conversely, Zhang et al demonstrated that miR-1246, under the regulation of p53, inhibited tumor growth in human hepatocellular carcinoma cells.[35] These seemingly contradictory findings actually reflect the multifaceted actions of miR-1246. As miRNAs can target a range of genes or proteins, their biological roles may differ across various tissues or cells.[36] Therefore, further exploration of the role of hsa-miR-1246 in lung cancer metastasis is essential to improve the reliability of the results.

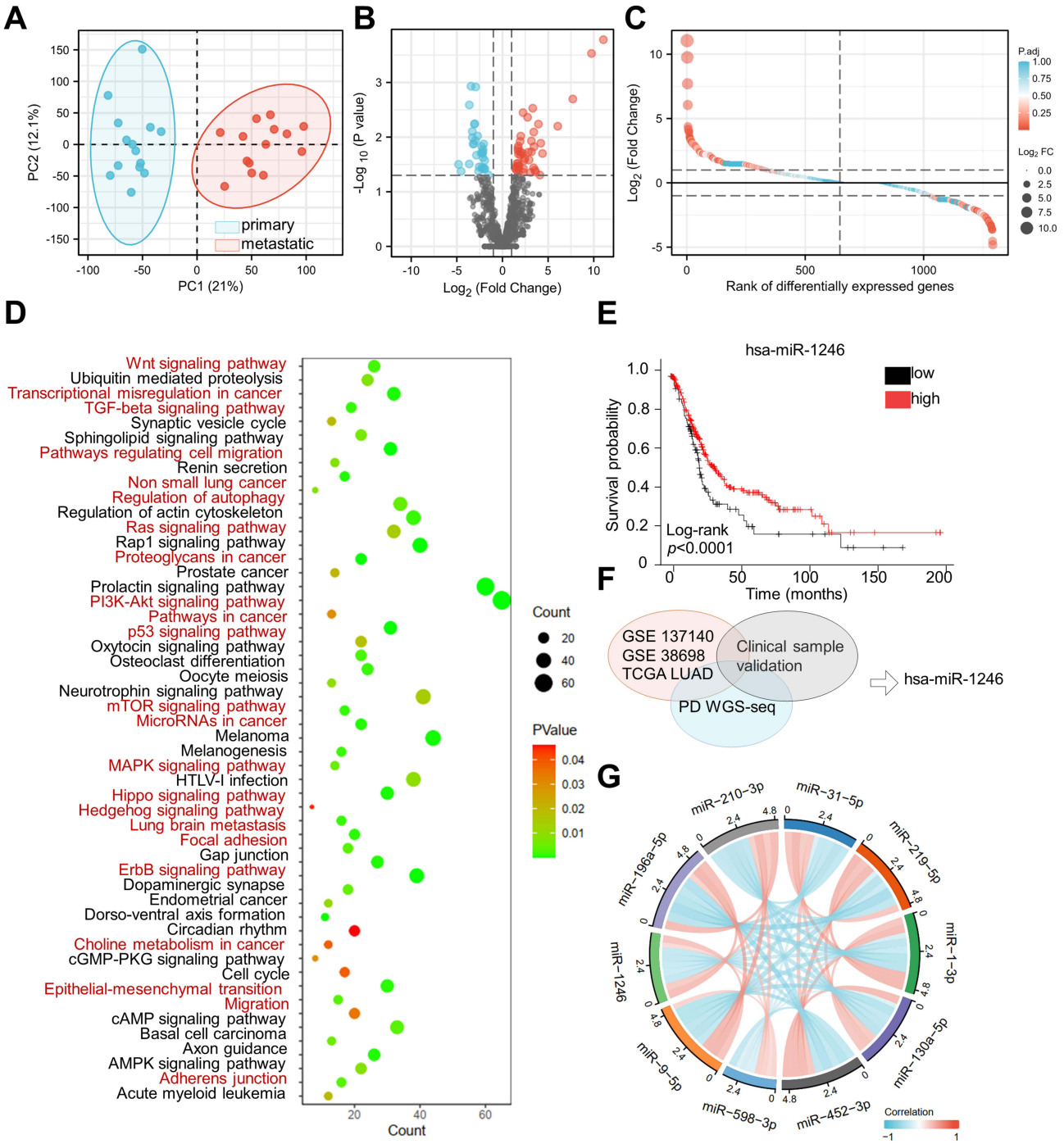

Figure 2 Identification of PD regulated microRNAs and its clinical significance. (**A**) Principal component analysis (PCA) is used to divide the primary lesions of lung cancer and metastases in the database. Blue dots represent the primary lesions of lung cancer and red dots represent metastatic lesions. (**B**) Volcano plot of differentially expressed miRNAs comparing the primary and metastatic sites. The data source is TCGA LUAD miRNA-seq data, and the red color is the upregulated miRNA in lung cancer metastasis sites compared to primary sites; blue is the downregulated miRNA in lung cancer metastasis sites compared to primary sites. (**C**) miRNA differential ranking plots. As shown in the figure, 1292 miRNAs were differentially expressed between the two groups. The parameters were set as |log2(FC)| > 2 and p.adj < 0.05, for which 27 miRNAs were highly expressed and 33 miRNAs were decreased compared to the primary sites of metastasis. (**D**) KEGG pathway analysis of the differentially expressed miRNAs. (**E**) Kaplan–Meier survival analysis of the effect of hsa-miR-1246 on the prognosis of lung cancer patients (HR = 0.71, P < 0.0001). (**F**) Differentially expressed miRNAs (DE-miRNAs) were comprehensively analyzed using the GEO database (GSE 137140, GSE 38698 dataset), TCGA LUAD database, whole-transcriptome analysis of PD, and clinical validation. (**G**) The Chord diagram illustrates the pairwise correlation of the 10 miRNAs selected from bioinformatics analysis.

https://doi.org/10.2147/IJN.S479675

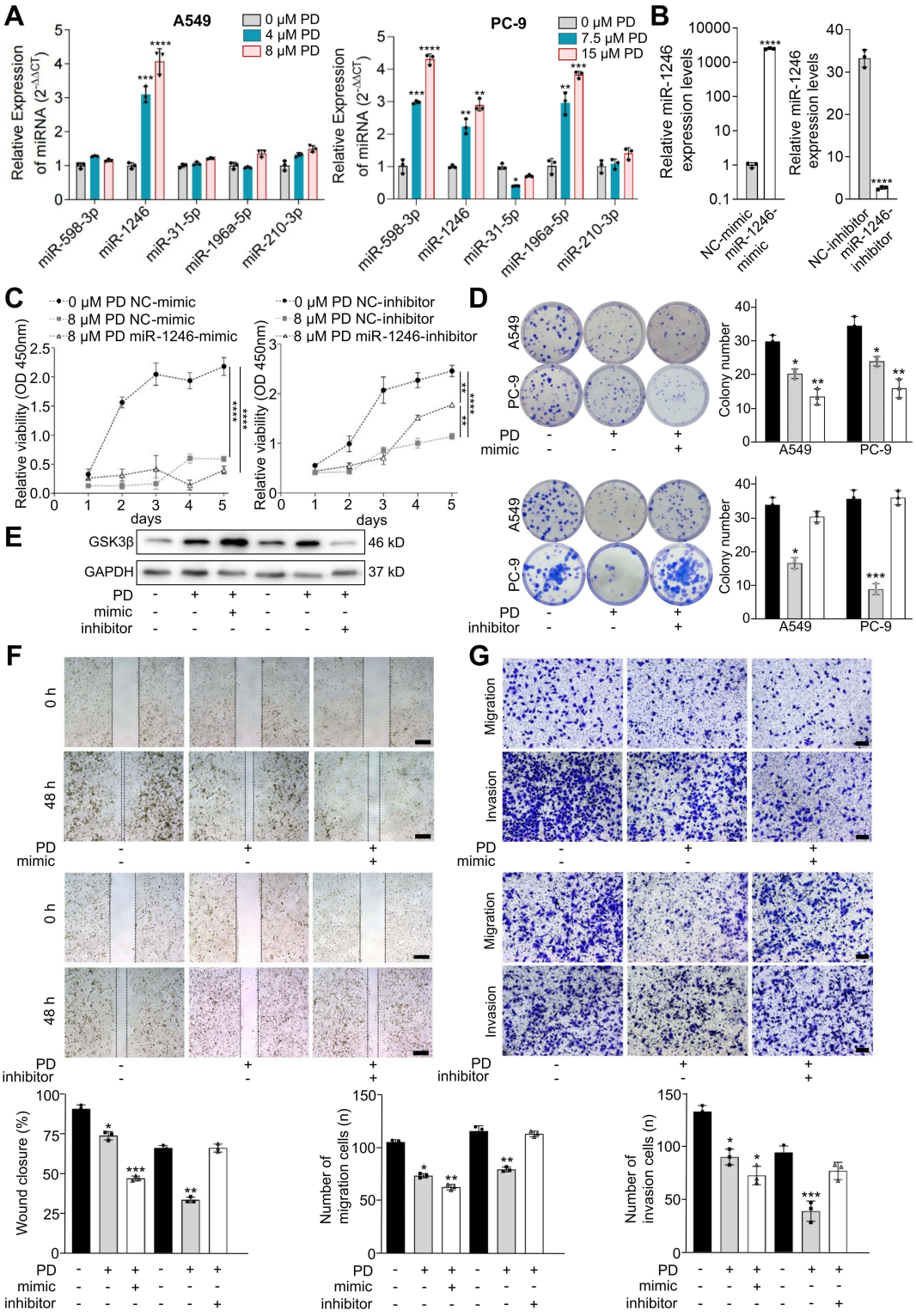

Figure 3 PD increases hsa-miR-1246 expression to mediate cell growth, migration, and invasion. (**A**) Qualitative PCR analysis of miRNA expression after PD treatment for 48h in different doses in A549 and PC-9 cells. N=3 for each group. (**B**) The influence of the expression of hsa-miR-1246 after transfection with the miR-1246-mimic and miR-1246-inhibitor for 48h. N=3 for each group. The effects of PD treatment combined with miR-1246-mimic and miR-1246-inhibitor transfection on (**C**) tumor growth and (**D**) colony formation. N=5 for each group. (**E**) The effects of PD treatment combined with miR-1246-mimic and miR-1246-inhibitor transfection on GSK3β expression. (**F**) Effect of different concentrations of PD combined with miR-1246-mimic and miR-1246-inhibitor transfection on the wound-healing function of A549 and PC-9 cells. N=3 for each group. Scale bar, 200 μm. (**G**) The effect of different concentrations of PD combined with miR-1246-mimic and miR-1246-inhibitor transfection on the migration and invasion of A549 and PC-9 cells. N=3 for each group. Scale bar, 100 μm. Data are shown as mean±SD, *P < 0.05, **P < 0.01, ***P < 0.001, ****P < 0.0001.

Hsa-miR-1246 Inhibits Cell Growth, Migration, and Invasion by Reducing FUT9

Employing target-prediction algorithms, we identified FUT9 as a potential direct target of the PD-regulated hsa-miR-1246. To validate this, we constructed luciferase reporter vectors containing the 3'-untranslated region (UTR) of FUT9 downstream of the luciferase genes, in both wild-type (WT) and mutant (MUT) configurations. The results indicated that Luciferase activity was significantly diminished by the WT vectors 01.03 and 05 (Figure 4A and B). This finding suggests that hsa-miR-1246 regulates FUT9 by directly binding to the FUT9 3'-UTR. Subsequent functional experiments confirmed that silencing FUT9 expression (shFUT9) attenuated tumor cell growth, migration, and invasion (Figure 4C–H).

In contrast, the overexpression of FUT9 (OE-FUT9) promoted tumor cell growth, migration, and invasion, as evidenced by wound healing and Transwell assays (Figure 5C–G). Additionally, OE-FUT9 exhibited increased expression in the Golgi apparatus, as revealed by confocal immunofluorescence co-localization with a Golgi-tracer, compared to the NC group (Figure 5A and B). In vivo, a higher number of metastatic sites were detected in the lungs, liver, and brain of mice in the OE-FUT9 group relative to the control group (Figure 5I). Futhermore, upregulation of FUT9 expression and downregulation of GSK3β expression in the lung tissue of the OE-FUT9 mice group were observed compared to the control (Figure 5H–J).

FUT9, a trans-Golgi and trans-Golgi network glycosyltransferase, is implicated in central nervous system maturation and acts as a metabolic driver in colorectal cancer progression.[37–39] Within neurons, FUT9 facilitates the transfer of fucose in an a3 linkage to terminal type II (Galb4GlcNAc) acceptors, which is the final step in the biosynthesis of the Lewis x (Lex) epitope.[40] In the colorectal cancer progression, FUT9 catalyzes the biosynthesis of Ley glycolipids, thereby promoting the proliferation of tumor-initiating cells.[41,42] Our study identified FUT9 as a contributor to NSCLC progression both in vitro and in vivo; however, its clinical relevance requires further investigation.

FUT9 Acts as an Oncogene During NSCLC Progression Through Single-Cell Sequencing Data Analysis

To investigate the clinical relevance of FUT9 in NSCLC, we acquired single-cell data from primary and metastatic NSCLC samples through NCBI's GEO database. We initiated our analysis with principal component analysis (PCA) on hypervariable genes in the dataset, which led to the identification of 25 subpopulations using ElbowPlot (Figure 6A). Utilizing SingleR, we annotated these subpopulations at the cell level based on tumor stage or cell type (Figure 6B and C). For gene level analysis, we employed the FindAllMarkers function to spotlight marker genes (GSK3β, β-catenin, and FUT9) among these subpopulations, with a significance threshold of a multiple difference of 0.5 and FDR < 0.05 (Figure 6D). Expression correlation analyses underscored the pivotal regulatory role of FUT9 in NSCLC metastasis (Figure 6E and F). Additionally, survival analysis indicated that a poor prognosis in NSCLC patients correlated with elevated FUT9 expression levels (Figure 6G). Collectively, these findings demonstrated that FUT9 is an important oncogene in NSCLC progression.

Homogenous Tumor Cell Membrane-Coated PD Delivery System could Attenuate the Hemolysis and Enhance the Therapeutic Effect in vivo

Bellflower saponins, including PD, possess hemolytic properties that can rupture red blood cells, making direct intravenous injection toxic.[43–45] Saponins interact with cholesterol on erythrocyte membranes, leading to membrane dissolution and reduced stability.[46,47] For oral administration, consume high levels of saponins, patients may experience uncomfortable gastrointestinal side effects such as abdominal pain, abdominal distension, diarrhea, bloating, nausea and vomiting.[48] To address this, we utilized homogeneous tumor cell membrane-functionalized drugs to improve pharmacokinetic profiles with a superior safety profile for PD and facilitate targeted delivery.[49–52]

To assess PD in vivo effectiveness, we developed a modified PD delivery system to minimize hemolytic toxicity. PD was encapsulated within A549 or PC-9 cell membranes to form PD@A549-m or PD@PC-9-m nanocomposites (Figure 7A). Transmission electron microscope (TEM) and dynamic light scattering (DLS) revealed uniform particle sizes with average diameters of 101 nm for A549-m, 123 nm for PC-9-m and 143 nm for PD@A549-m. TEM also

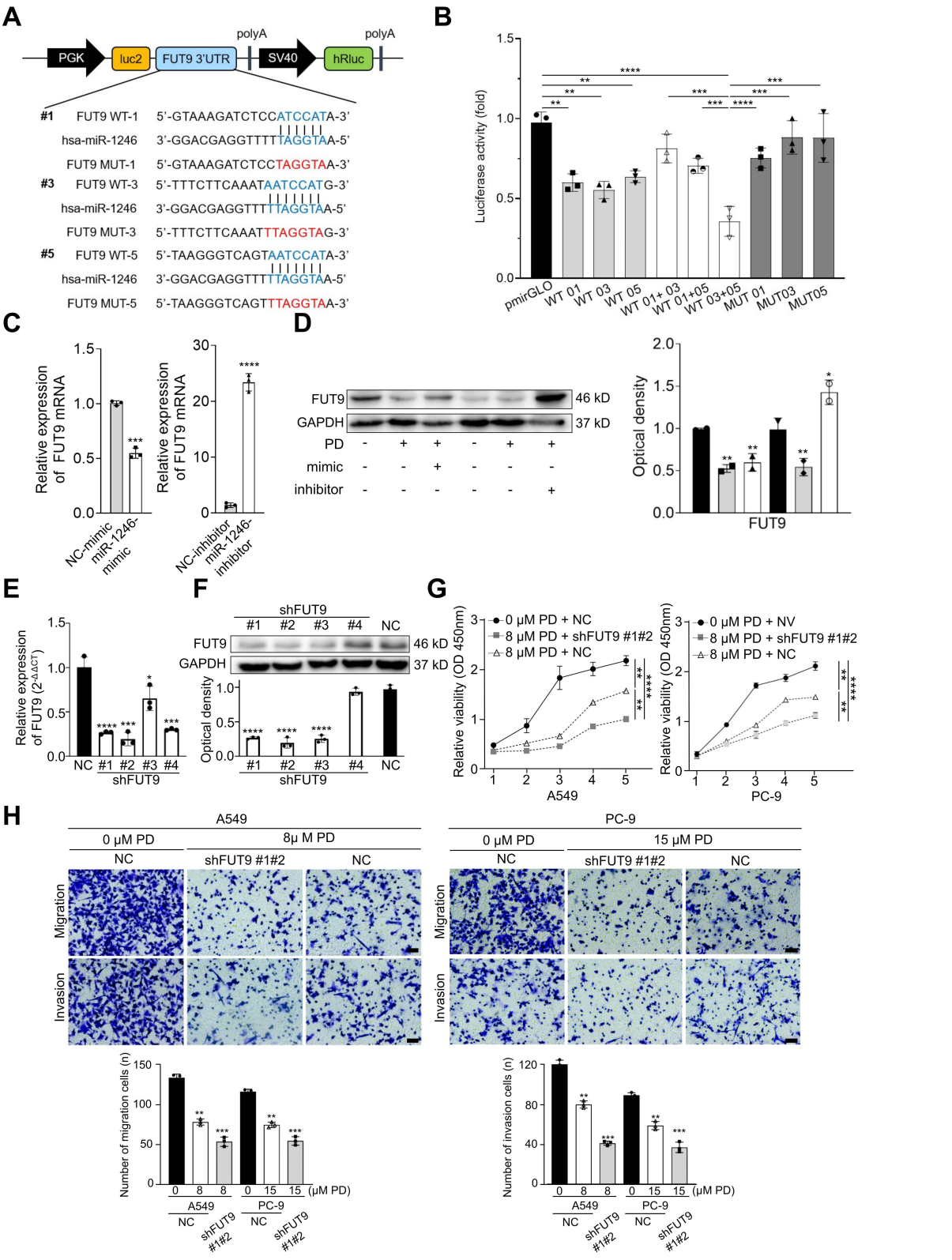

Figure 4 Hsa-miR-1246 inhibits cell growth, migration, and invasion by reducing FUT9. (**A**) The specific binding sites of hsa-miR-1246 and FUT9 were analyzed using the TargetScan database, and three corresponding mutation sites were designed. (**B**) The luciferase signal of FUT9 in 293T cells was detected using a dual-luciferase reporter gene assay. N=3 for each group. (**C** and **D**) The effects of PD treatment combined with miR-1246-mimic and miR-1246-inhibitor transfection on FUT9 expression. N=3 for each group. (**E** and **F**) Silencing sites of FUT9 were designed and validated using qRT-PCR and Western blot analysis. N=3 for each group. (**G**) Synergistic inhibitory effects of PD and shFUT9 on cell growth. N=5 for each group. (**H**) Synergistic inhibitory effects of PD and shFUT9 on cell migration and invasion. N=3 for each group. Scale bar, 100 μm. Data are shown as mean ± SD, *P < 0.05, **P < 0.01, ***P < 0.001, ****P < 0.0001.

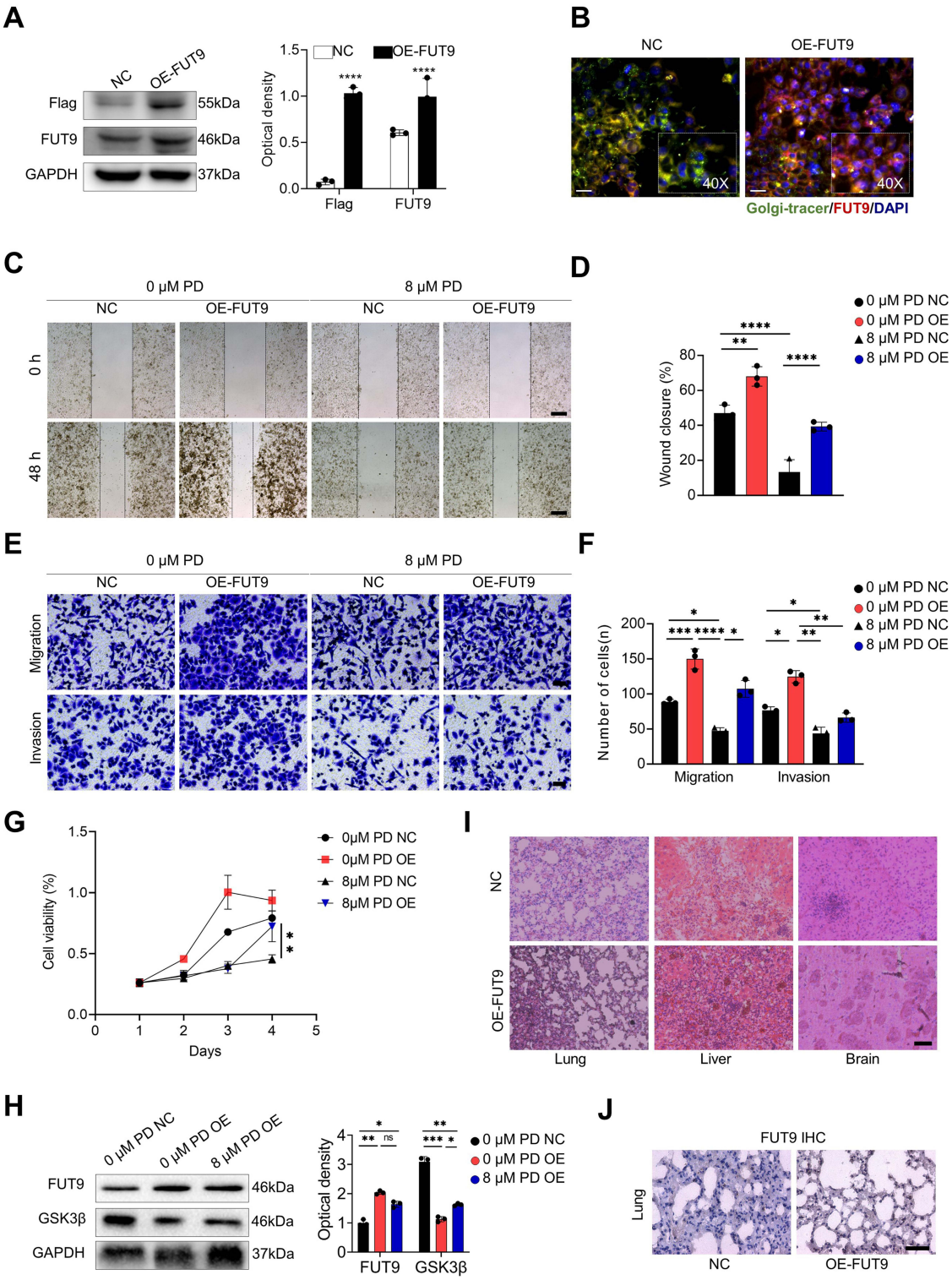

Figure 5 Overexpression of FUT9 could promote the NSCLC progression both in vitro and in vivo. (**A**) Validation of overexpression (OE)-FUT9 vector. N=3 for each group. (**B**) Representative confocal fluorescence imaging of a Golgi tracer (in green) and FUT9 (in red) showing the characteristic location of FUT9 in the Golgi in OE-FUT9 A549 cells. Scale bar, 50 μm. (**C** and **D**) The wound-healing assay demonstrated that OE-FUT9 could rescue the inhibitory effect of PD on cell migration. N=3 for each group. Scale bar, 200 μm. (**E** and **F**) Transwell assays demonstrated that OE-FUT9 rescued the inhibitory effect of PD on cell migration and invasion. N=3 for each group. Scale bar, 100 μm. (**G**) The CCK-8 assay demonstrated that OE-FUT9 rescued the inhibition of PD on cell growth. N=5 for each group. (**H**) In vivo expression changes in FUT9 and GSK3β in mice injected with OE-FUT9 cells compared to mice injected with NC cells. N=3 for each group. (**I**) Hematoxylin and eosin (H&E) staining of FUT9 in the lung, liver, and brain tissues of mice injected with OE-FUT9 cells compared with mice injected with NC cells. Scale bar, 100 μm. (**J**) Representative images of immunohistochemistry (IHC) staining of FUT9 in lung tissues of mice injected with OE-FUT9 cells compared to mice injected with NC cells. Scale bar, 100 μm. Data are shown as mean±SD, *P < 0.05, **P < 0.01, ***P < 0.001, ****P < 0.0001.

https://doi.org/10.2147/IJN.S479675

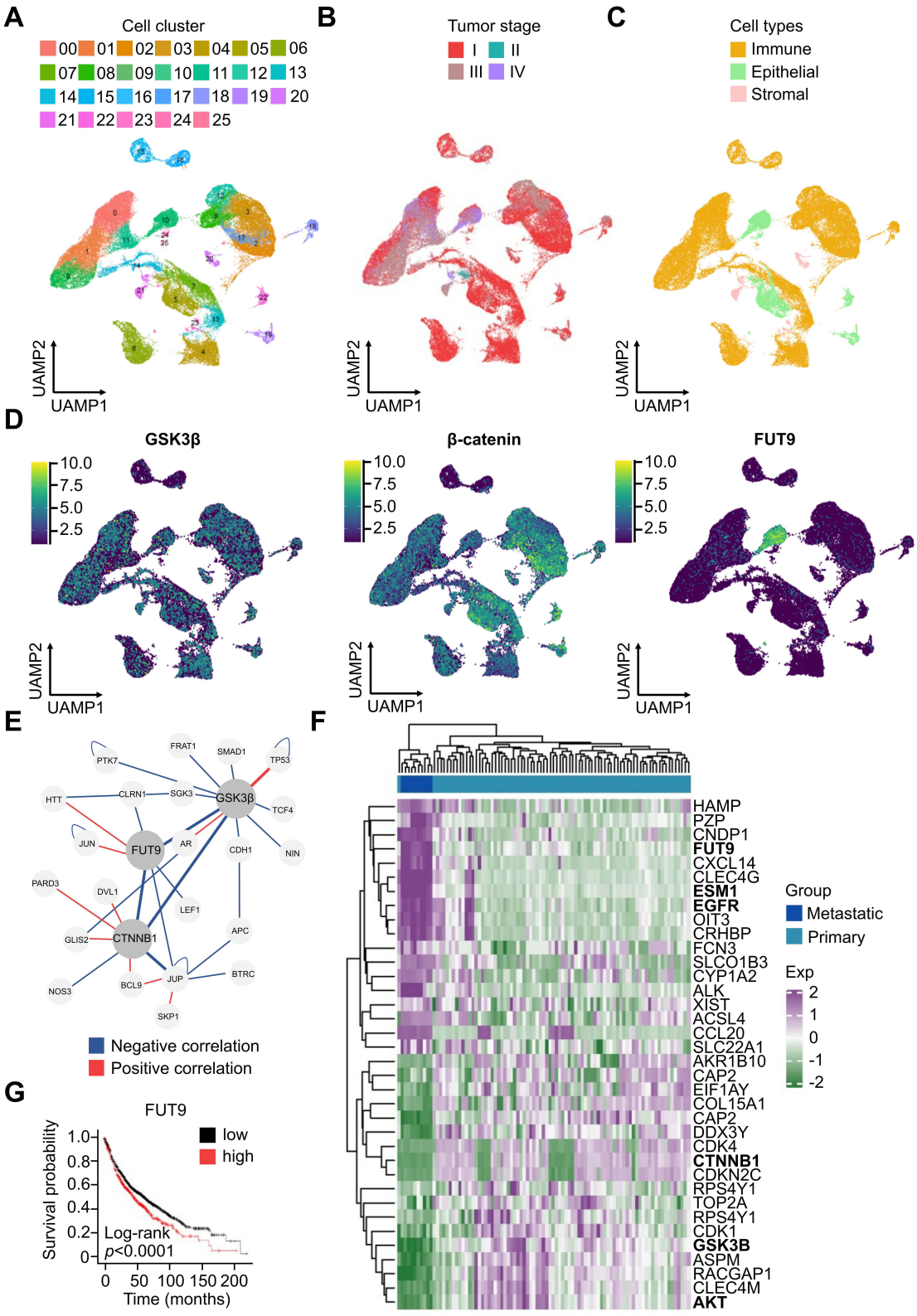

Figure 6 FUT9 acts as an oncogene during NSCLC progression through single-cell sequencing data analysis. (**A**) Principal component analysis (PCA) using hypervariable genes from the GEO dataset. (**B** and **C**) Subgroups were annotated according to tumor stage or cell leveraging SingleR. (**D**) Gene-level analysis using the FindAllMarkers function with a multiple difference of 0.5, FDR < 0.05. (**E** and **F**) Correlation analysis of FUT9, GSK3β, β-catenin, and other genes. (**G**) Kaplan–Meier survival analysis of FUT9 on the prognosis of patients with lung cancer.

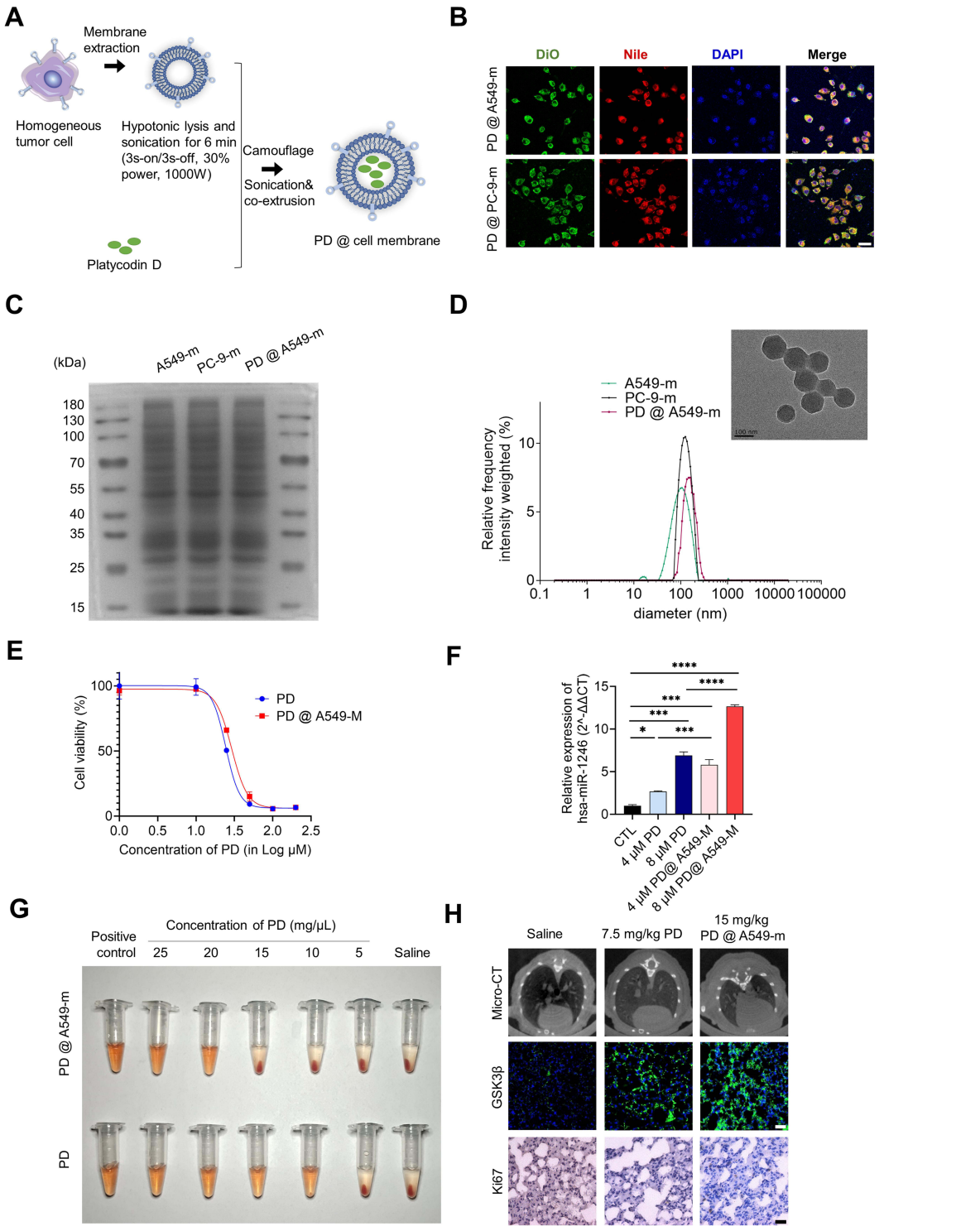

Figure 7 Homogenous tumor cell membrane-coated PD delivery system could attenuate the hemolysis and enhance the therapeutic effect in vivo. (**A**) Schematic diagram of homogenous tumor cell membrane-coated PD delivery system. A549 or PC-9 cells were cultured in 150 mm cell culture dishes, and 2×10^8 cells were counted. After the cells were completely digested with a cell scraper, they were centrifuged at 400 × g for 5 min, washed with PBS, and centrifuged at 400 × g for 5 min. Then 4 × volume of hypotonic buffer containing protease inhibitors was added, followed by shaking every 15 min on ice to disrupt the cells. After 1 h, the cells were disrupted by sonication for 6 min (3s-on / 3s-off, 30% power, 1000 W. The suspension was then centrifuged machine at 15000 g at 4 °C for 30 min using a high-speed centrifuge, and the supernatant was collected and extruded through a 200 nm pore-sized polycarbonate membrane several times to obtain cell membrane fragments with a relatively uniform particle size. (**B**) Representative images of NSCLC cells co-cultivated with PD@A549-m or PD@PC-9-m for 48 h. Scale bar, 50 μm. (**C**) SDS-PAGE and Coomassie Brilliant Blue staining of A549 (A549-m), PC-9 (PC-9-m), and PD@A549-m cell membranes. (**D**) The size and morphology of the synthesized particles were characterized using DLS and TEM. Scale bar, 100 nm. (**E**) The effect of PD@A549-m on A549 cell growth. N=5 for each group. (**F**) The effect of PD@A549-m on hsa-miR-1246 expression. N=3 for each group. (**G**) Hemolytic effect of PD and PD@A549-m on red blood cells. (**H**) Effect of PD and PD@A549-m administration on lung tumor growth in mice. Scale bar, 50 μm. Data are shown as mean±SD, *P < 0.05, ***P < 0.001, ****P < 0.0001.

https://doi.org/10.2147/IJN.S479675

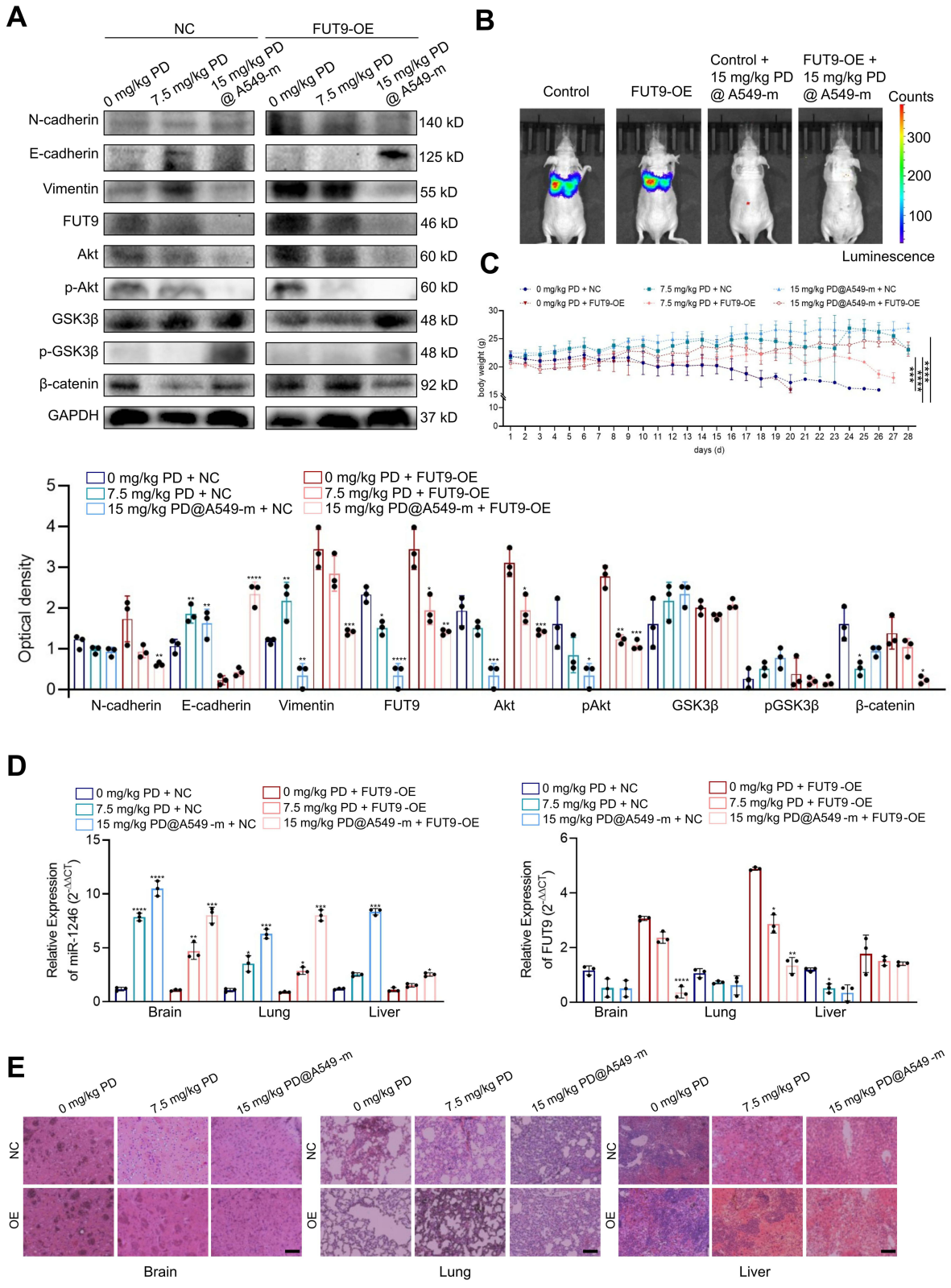

Figure 8 PD inhibits the NSCLC metastasis through hsa-miR-1246/FUT9/ GSK3β pathway in vivo. (**A**) Effect of PD and FUT9-OE on protein expression in mouse lung tissue. N=3 for each group. (**B**) In vivo bioluminescence imaging of the animals. (**C**) Body weight changes in mice in the different treatment groups. N=3 for each group. (**D**) The effect of PD and FUT9-OE on hsa-miR-1246 expression in the lung, liver, and brain tissues of mice. N=3 for each group. (**E**) Representative tissue sections were stained with hematoxylin and eosin (H&E). Scale bar, 100 μm. *P < 0.05, **P < 0.01, ***P < 0.001, ****P < 0.0001.

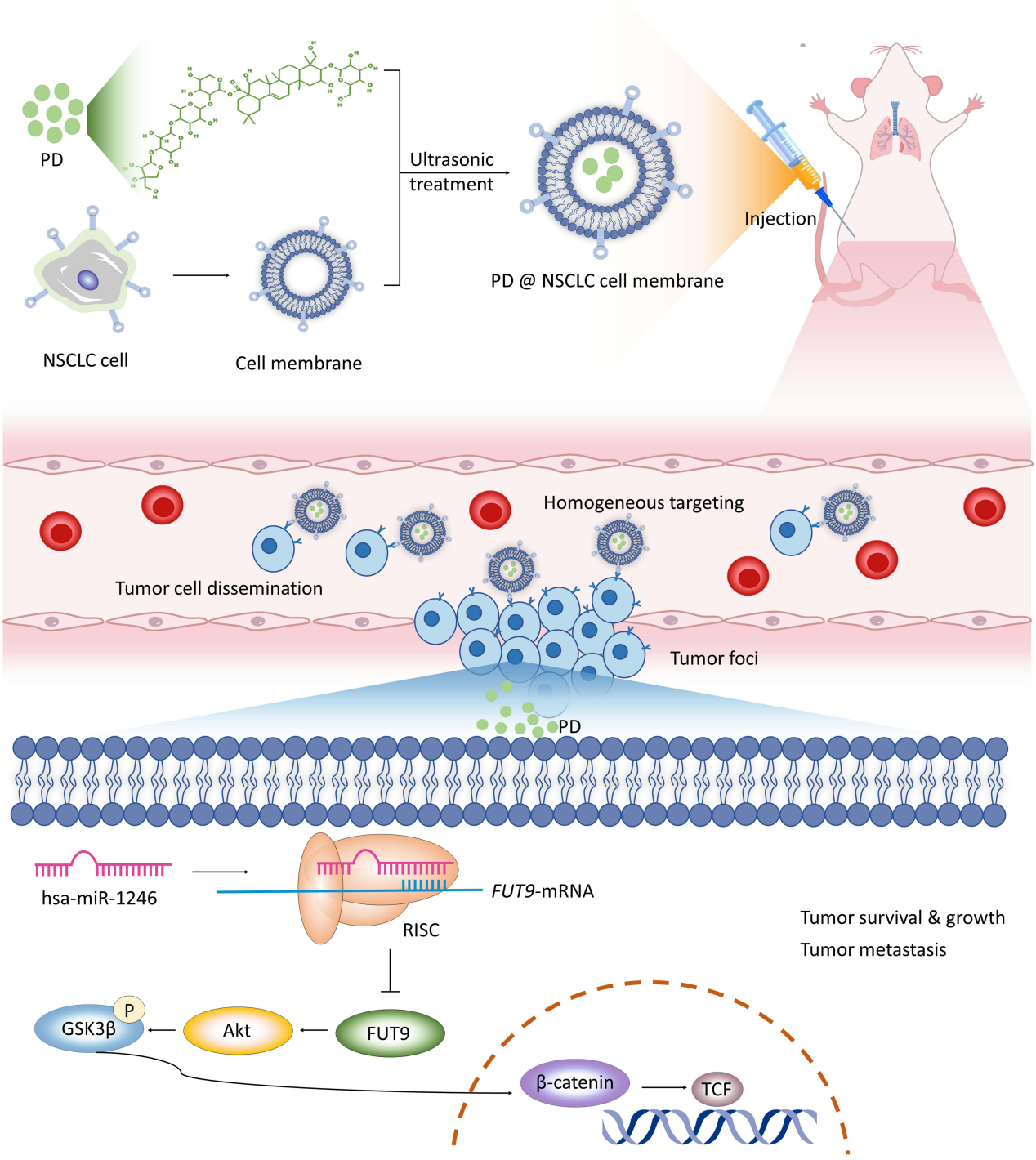

Scheme 1 Schematic illustrating potential mechanism that PD inhibit NSCLC progression via regulating hsa-miR-1246/FUT9/GSK3β pathway.

confirmed the "shell-core" structure formed by membrane wrapping, indicating successful coating of PD with the homogenous tumor cell membrane (Figure 7D). SDS-PAGE showed the retention of cell surface proteins (Figure 7C). Uptake studies showed that NSCLC cells efficiently internalized the coated PD, with 87% efficiency for PD@A549-m and 92% for PD@PC-9-m after 48 h of co-culture (Figure 7B and Supplementary Figure S2). Moreover, PD and PD@A549-m exhibited similar inhibitory effects on tumor cell growth and regulation of hsa-miR -1246, demonstrating the preservation of biological functions in the tumor cell membrane-coated PD delivery system (Figure 7E and F). Hemolysis assays showed no hemolysis induced by PD@A549-m even at

https://doi.org/10.2147/IJN.S479675

a concentration of 15 mg/μL, exceeding the hemolysis threshold for PD (Figure 7G). Therefore, the homogenous tumor cell membrane-coated delivery system neutralized the hemolytic toxicity of PD by 75%, enhancing its safety for in vivo use (Supplementary Figure S3). In a lung tumor metastasis mouse model, the tumor nodules of mice in the PD@A549-m administration group were 29% less than those in the PD administration group and 51% less than those in the control group, indicating effective inhibition of tumor metastasis by PD@A549-m in vivo. Furthermore, a decrease in Ki-67 expression and an increase in GSK3β expression were observed in the PD@A549-m group relative to the PD and control groups (Figure 7H).

PD Inhibits the NSCLC Metastasis Through Hsa-miR-1246/FUT9/GSK3β Pathway in vivo

Based on the aforementioned findings, we have further elucidated the mechanism by which PD suppresses tumor growth and metastasis by regulating the hsa-miR-1246/FUT9/ GSK3β pathway in vivo. Mice in the FUT9-OE group exhibited highly progressive characteristics such as increased levels of N-cadherin, vimentin, Akt, phosphorylated-Akt, and β-catenin, and decreased levels of E-cadherin, GSK3β, and phosphorylated-GSK3β, compared to the control group. This phenotype was reserved by the administration of PD or PD@A549-m (Figure 8A). Through in vivo bioluminescent imaging, a reduction in lung tumor growth was observed in the PD@A549-m treatment group relative to the saline control group, as assessed in a lung cancer metastasis model (Figure 8B). Moreover, body weight changes corroborated the therapeutic efficacy of PD in vivo (Figure 8C). Consistent with cellular observations, the expression levels of hsa-miR-1246 in brain, lung, and liver tissues post-sacrifice mirrored the trend seen in cellular studies (Figure 8D). Histological examination of metastatic lesions within the lung, brain, and liver tissues confirmed significant suppression of metastases in the lung and brain tissues under treatment (Figure 8E).

Conclusions

The present study demonstrated the inhibitory effects of PD on tumor growth, migration, and invasion, both in vitro and in vivo. Treatment with PD led to the upregulation of hsa-miR-1246 and the downregulation of FUT9 expression. Furthermore, the efficacy and safety of PD therapy in vivo were significantly improved by employing a homogenous tumor cell membrane-coated delivery system. These results suggest a promising role for PD in controlling the progression of NSCLC (Scheme 1).

Data Sharing Statement

Please contact the corresponding author for all data requests.

Acknowldegments

We thank Prof. Yang Zhao for assistance in HUVEC cultivation and technical support for in vivo imaging of small animals by Dr. Zuoxiu Tie from Nanjing University.

Author Contributions

All authors made a significant contribution to the work reported, whether that is in the conception, study design, execution, acquisition of data, analysis and interpretation, or in all these areas; took part in drafting, revising or critically reviewing the article; gave final approval of the version to be published; have agreed on the journal to which the article has been submitted; and agree to be accountable for all aspects of the work.

Funding

This research was funded by the National Natural Science Foundation of China, grant number 82004081, 52073145, and the National Natural Science Foundation of Nanjing University of Chinese Medicine, grant number NZY82004081.

Disclosure

The authors declare no competing interests in this work.

References

1. Sung H, Ferlay J, Siegel RL. et al. Global cancer statistics 2020: GLOBOCAN estimates of incidence and mortality worldwide for 36 cancers in 185 countries. *CA Cancer J Clin*. 2021;71(3):209–249. doi:10.3322/caac.21660
2. Duma N, Santana-Davila R, Molina JR. Non-small cell lung cancer: epidemiology, screening, diagnosis, and treatment. *Mayo Clin Proc*. 2019;94(8):1623–1640. doi:10.1016/j.mayocp.2019.01.013
3. Altorki NK, Markowitz GJ, Gao D, et al. The lung microenvironment: an important regulator of tumour growth and metastasis. *Nat Rev Cancer*. 2019;19(1):9–31. doi:10.1038/s41568-018-0081-9
4. Jasper K, Stiles B, McDonald F, Palma DA. Practical management of oligometastatic non-small-cell lung cancer. *J Clin Oncol*. 2022;40(6):635–641. doi:10.1200/JCO.21.01719
5. Achrol AS, Rennert RC, Anders C, et al. Brain metastases. *Nat Rev Dis Primers*. 2019;5(1):5. doi:10.1038/s41572-018-0055-y
6. Lou JS, Zhao LP, Huang ZH, et al. Ginkgetin derived from Ginkgo biloba leaves enhances the therapeutic effect of cisplatin via ferroptosis-mediated disruption of the Nrf2/HO-1 axis in EGFR wild-type non-small-cell lung cancer. *Phytomedicine*. 2021;80:153370. doi:10.1016/j.phymed.2020.153370
7. Li Z, Feiyue Z, Gaofeng L. Traditional Chinese medicine and lung cancer--From theory to practice. *Biomed Pharmacother*. 2021;137:111381. doi:10.1016/j.biopha.2021.111381
8. Zhang W, Tian W, Wang Y, et al. Explore the mechanism and substance basis of Mahuang FuziXixin Decoction for the treatment of lung cancer based on network pharmacology and molecular docking. *Comput Biol Med*. 2022;151(Pt A):106293. doi:10.1016/j.compbiomed.2022.106293
9. Wang X, Hou L, Cui M, Liu J, Wang M, Xie J. The traditional Chinese medicine and non-small cell lung cancer: from a gut microbiome perspective. *Front Cell Infect Microbiol*. 2023;13:1151557. doi:10.3389/fcimb.2023.1151557
10. Wei Z, Chen J, Zuo F, et al. Traditional Chinese Medicine has great potential as candidate drugs for lung cancer: a review. *J Ethnopharmacol*. 2023;115748. doi:10.1016/j.jep.2022.115748
11. Chen S, Wang Q, Ming S, Zheng H, Hua B, Yang HS. Platycodin D induces apoptosis through JNK1/AP-1/PUMA pathway in non-small cell lung cancer cells: a new mechanism for an old compound. *Front Pharmacol*. 2022;13:1045375. doi:10.3389/fphar.2022.1045375
12. Hu X, Fu Y, Lu X, et al. Protective Effects of Platycodin D on Lipopolysaccharide-Induced Acute Lung Injury by Activating LXRα-ABCA1 Signaling Pathway. *Front Immunol*. 2017;7:644. doi:10.3389/fimmu.2016.00644
13. Khan M, Maryam A, Zhang H, Mehmood T, Ma T. Killing cancer with platycodin D through multiple mechanisms. *J Cell Mol Med*. 2016;20(3):389–402. doi:10.1111/jcmm.12749
14. Xie L, Zhao YX, Zheng Y, Li XF. The pharmacology and mechanisms of platycodin D, an active triterpenoid saponin from Platycodon grandiflorus. *Front Pharmacol*. 2023;14:1148853. doi:10.3389/fphar.2023.1148853
15. Huang MY, Jiang XM, Xu YL, et al. Platycodin D triggers the extracellular release of programed death Ligand-1 in lung cancer cells. *Food Chem Toxicol*. 2019;131:110537. doi:10.1016/j.fct.2019.05.045
16. Son JA, Lee SK, Park J, et al. Platycodin D Inhibits Vascular Endothelial Growth Factor-Induced Angiogenesis by Blocking the Activation of Mitogen-Activated Protein Kinases and the Production of Interleukin-8. *Am J Chin Med*. 2022;50(6):1645–1661. doi:10.1142/S0192415X22500690
17. Li T, Xu XH, Tang ZH, et al. Platycodin D induces apoptosis and triggers ERK- and JNK-mediated autophagy in human hepatocellular carcinoma BEL-7402 cells. *Acta Pharmacol Sin*. 2015;36(12):1503–1513. doi:10.1038/aps.2015.99
18. Zheng S, Xie Z, Xin Y, et al. Whole Transcriptome Analysis Identifies Platycodin D-Mediated RNA Regulatory Network in Non-Small-Cell Lung Cancer. *Cells*. 2022;11(15):2360. doi:10.3390/cells11152360
19. Sell MC, Ramlogan-Steel CA, Steel JC, Dhungel BP. MicroRNAs in cancer metastasis: biological and therapeutic implications. *Expert Rev Mol Med*. 2023;17:25:e14.
20. Urbanek-Trzeciak MO, Galka-Marciniak P, Nawrocka PM, et al. Pan-cancer analysis of somatic mutations in miRNA genes. *EBioMedicine*. 2020;61:103051. doi:10.1016/j.ebiom.2020.103051
21. Iqbal MA, Arora S, Prakasam G, Calin GA, Syed MA. MicroRNA in lung cancer: role, mechanisms, pathways and therapeutic relevance. *mol Aspects Med*. 2019;70:3–20. doi:10.1016/j.mam.2018.07.003
22. Davenport ML, Echols JB, Silva AD, et al. miR-31 Displays Subtype Specificity in Lung Cancer. *Cancer Res*. 2021;81(8):1942–1953. doi:10.1158/0008-5472.CAN-20-2769
23. Zhu C, Wang S, Zheng M, et al. miR-31-5p modulates cell progression in lung adenocarcinoma through TNS1/p53 axis. *Strahlenther Onkol*. 2022;198(3):304–314. doi:10.1007/s00066-021-01895-x
24. Dai S, Li F, Xu S, Hu J, Gao L. The important role of miR-1-3p in cancers. *J Transl Med*. 2023;21(1):769. doi:10.1186/s12967-023-04649-8
25. Li T, Wang X, Jing L, Li Y. MiR-1-3p inhibits lung adenocarcinoma cell tumorigenesis via targeting protein regulator of cytokinesis 1. *Front Oncol*. 2019;9:120. doi:10.3389/fonc.2019.00120
26. Miao H, Zeng Q, Xu S, Chen Z. miR-1-3p/CELSR3 participates in regulating malignant phenotypes of lung adenocarcinoma cells. *Curr Gene Ther*. 2021;21(4):304–312. doi:10.2174/1566523221666210617160611
27. Zhu MC, Zhang YH, Xiong P, Fan XW, Li GL, Zhu M. Circ-GSK3B up-regulates GSK3B to suppress the progression of lung adenocarcinoma. *Cancer Gene Ther*. 2022;29(11):1761–1772. doi:10.1038/s41417-022-00489-8
28. Thanee M, Dokduang H, Kittirat Y, et al. CD44 modulates metabolic pathways and altered ROS-mediated Akt signal promoting cholangiocarcinoma progression. *PLoS One*. 2021;16(3):e0245871. doi:10.1371/journal.pone.0245871
29. Anders S, Huber W. Differential expression analysis for sequence count data. *Genome Biol*. 2010;11(10):R106. doi:10.1186/gb-2010-11-10-r106
30. Robinson MD, McCarthy DJ, Smyth GK. edgeR: a Bioconductor package for differential expression analysis of digital gene expression data. *Bioinformatics*. 2010;26(1):139–140. doi:10.1093/bioinformatics/btp616
31. Wang Z, Gao D, Wang S, Lin H, Wang Y, Xu W. Exosomal microRNA-1246 from human umbilical cord mesenchymal stem cells potentiates myocardial angiogenesis in chronic heart failure. *Cell Biol Int*. 2021;45(11):2211–2225. doi:10.1002/cbin.11664

32. Huang JL, Fu YP, Gan W, et al. Hepatic stellate cells promote the progression of hepatocellular carcinoma through microRNA-1246-RORα-Wnt/β-Catenin axis. *Cancer Lett*. 2020;476:140–151. doi:10.1016/j.canlet.2020.02.012
33. Yang F, Xiong H, Duan L, Li Q, Li X, Zhou Y. MiR-1246 promotes metastasis and invasion of A549 cells by targeting GSK-3β–mediated Wnt/β-catenin pathway. *Cancer Res Treat*. 2019;51(4):1420–1429. doi:10.4143/crt.2018.638
34. Yuan D, Xu J, Wang J, et al. Extracellular miR-1246 promotes lung cancer cell proliferation and enhances radioresistance by directly targeting DR5. *Oncotarget*. 2016;7(22):32707–32722. doi:10.18632/oncotarget.9017
35. Zhang Q, Cao LY, Cheng SJ, Zhang AM, Jin XS, Li Y. p53-induced microRNA-1246 inhibits the cell growth of human hepatocellular carcinoma cells by targeting NFIB. *Oncol Rep*. 2015;33(3):1335–1341. doi:10.3892/or.2015.3715
36. Ghafouri-Fard S, Khoshbakht T, Hussen BM, Taheri M, Samadian M. A review on the role of miR-1246 in the pathoetiology of different cancers. *Front Mol Biosci*. 2022;8:771835. doi:10.3389/fmolb.2021.771835
37. Zheng W, He R, Liang X, et al. Cell-specific targeting of extracellular vesicles through engineering the glycocalyx. *J Extracell Vesicles*. 2022;11 (12):e12290. doi:10.1002/jev2.12290
38. Nishihara S, Iwasaki H, Nakajima K, et al. Alpha1,3-fucosyltransferase IX (Fut9) determines Lewis X expression in brain. *Glycobiology*. 2003;13 (6):445–455. doi:10.1093/glycob/cwg048
39. Kudo T, Kaneko M, Iwasaki H, et al. Normal embryonic and germ cell development in mice lacking alpha 1,3-fucosyltransferase IX (Fut9) which show disappearance of stage-specific embryonic antigen 1. *Mol Cell Biol*. 2004;24(10):4221–4228. doi:10.1128/MCB.24.10.4221-4228.2004
40. Noro E, Togayachi A, Sato T, et al. Large-scale identification of N-glycan glycoproteins carrying Lewis x and site-specific N-glycan alterations in fut9 knockout mice. *J Proteome Res*. 2015;14(9):3823–3834. doi:10.1021/acs.jproteome.5b00178
41. Auslander N, Cunningham CE, Toosi BM, et al. An integrated computational and experimental study uncovers FUT9 as a metabolic driver of colorectal cancer. *mol Syst Biol*. 2017;13(12):956. doi:10.15252/msb.20177739
42. Blanas A, Zaal A, van der Haar Àvila I, et al. FUT9-driven programming of colon cancer cells towards a stem cell-like state. *Cancers*. 2020;12 (9):2580. doi:10.3390/cancers12092580
43. Lee DJ, Choi JW, Kang JN, Lee SM, Park GH, Kim CK. Chromosome-scale genome assembly and triterpenoid saponin biosynthesis in Korean bellflower (Platycodon grandiflorum). *Int J mol Sci*. 2023;24(7):6534. doi:10.3390/ijms24076534
44. Manaargadoo-Catin M, Ali-Cherif A, Pougnas JL, Perrin C. Hemolysis by surfactants--A review. *Adv Colloid Interface Sci*. 2016;228:1–16. doi:10.1016/j.cis.2015.10.011
45. Lorent JH, Quetin-Leclercq J, Mingeot-Leclercq MP. The amphiphilic nature of saponins and their effects on artificial and biological membranes and potential consequences for red blood and cancer cells. *Org Biomol Chem*. 2014;12(44):8803–8822. doi:10.1039/C4OB01652A
46. Liao Y, Li Z, Zhou Q, et al. Saponin surfactants used in drug delivery systems: a new application for natural medicine components. *Int J Pharm*. 2021;603:120709. doi:10.1016/j.ijpharm.2021.120709
47. Sarikahya NB, Nalbantsoy A, Top H, Gokturk RS, Sumbul H, Kirmizigul S. Immunomodulatory, hemolytic and cytotoxic activity potentials of triterpenoid saponins from eight Cephalaria species. *Phytomedicine*. 2018;1:135–144. doi:10.1016/j.phymed.2017.11.009
48. Huang H, Wu D, Li Q, et al. Jiegeng decoction ameliorated acute pharyngitis through suppressing NF-κB and MAPK signaling pathways. *J Ethnopharmacol*. 2024;332:118328. doi:10.1016/j.jep.2024.118328
49. Guo W, Liu W, Wan P, et al. Cationic amphiphilic dendrons with anticancer activity. *ACS Biomater Sci Eng*. 2022;8(5):2121–2130. doi:10.1021/acsbiomaterials.2c00181
50. Sun Y, Zhai W, Liu X, et al. Homotypic cell membrane-cloaked biomimetic nanocarrier for the accurate photothermal-chemotherapy treatment of recurrent hepatocellular carcinoma. *J Nanobiotechnol*. 2020;18(1):60. doi:10.1186/s12951-020-00617-2
51. Fang RH, Gao W, Zhang L. Targeting drugs to tumours using cell membrane-coated nanoparticles. *Nat Rev Clin Oncol*. 2023;20(1):33–48. doi:10.1038/s41571-022-00699-x
52. Szlasa W, Zendran I, Zalesińska A, Tarek M, Kulbacka J. Lipid composition of the cancer cell membrane. *J Bioenerg Biomembr*. 2020;52 (5):321–342. doi:10.1007/s10863-020-09846-4